Spin-wave nonreciprocity and formation of lateral standing spin waves in CoFeB/Ta/NiFe meander-shaped films ⊘

Special Collection: Recent Advances in Magnonics

G. Gubbiotti ✉; A. Sadovnikov; S. E. Sheshukova; ... et. al

Check for updates

View Online   Export Citation   CrossMark

Articles You May Be Interested In

Magnonic band structure in CoFeB/Ta/NiFe meander-shaped magnetic bilayers

Appl. Phys. Lett. (April 2021)

Nonreciprocal behavior of the spin pumping in ultra-thin film of CoFeB

Journal of Applied Physics (April 2016)

Cu spacer layer dependence of magneto-impedance effect in electrodeposited multilayered $[NiFe/Cu/NiFe]_3/Cu/[NiFe/Cu/NiFe]_3$

AIP Conference Proceedings (May 2023)

Spin-wave nonreciprocity and formation of lateral standing spin waves in CoFeB/Ta/NiFe meander-shaped films

G. Gubbiotti,[1,a] A. Sadovnikov,[2] S. E. Sheshukova,[2] E. Beginin,[2] S. Nikitov,[2,3,4] G. Talmelli,[5] C. Adelmann,[5] and F. Ciubotaru[5]

AFFILIATIONS

[1]Istituto Officina dei Materiali del CNR (CNR-IOM), c/o Dipartimento di Fisica e Geologia, Università di Perugia, I-06123 Perugia, Italy
[2]Laboratory Magnetic Metamaterials, Saratov State University, 83 Astrakhanskaya Street, Saratov 410012, Russia
[3]Kotel'nikov Institute of Radioengineering and Electronics, Russian Academy of Sciences, Moscow 125009, Russia
[4]Terahertz Spintronics Laboratory, Moscow Institute of Physics and Technology (National University), 9 Institutskii lane, Dolgoprudny 141700, Russia
[5]Imec, 3001 Leuven, Belgium

Note: This paper is part of the Special Topic on Recent Advances in Magnonics.
[a]**Author to whom correspondence should be addressed:** gubbiotti@iom.cnr.it

ABSTRACT

Studying the spin-wave (SW) propagation in 3D periodic structures opens new possibilities for joining functional units placed on the different layers of the magnonic circuitry. In the path toward 3D magnonics, the main *challenge is the fabrication* of large-scale 3D magnetic structures with nanometric precision control of geometry and material composition. In this work, we study the dependence on the Ta spacer thickness of the magnonic band structure, measured by Brillouin light scattering spectroscopy, of CoFeB/Ta/NiFe meander-shaped bilayers fabricated on pre-patterned Si substrate with thickness steps of 50 nm. Both propagating and stationary SW modes are observed. While the frequency of the dispersive mode slightly depends on the Ta spacer thickness, the frequency position of the three stationary modes in the lowest frequency range of the spectra significantly increases by increasing the Ta thickness. Micromagnetic calculations indicate that each of the three stationary modes is composed of a doublet of modes whose frequency separation, within each doublet, increases by increasing the mode frequency. The origin of this frequency separation is ascribed to the dynamic dipolar coupling between the magnetic layers that generate a significant frequency nonreciprocity of counterpropagating SWs. For these reasons, the investigated structures offer potential application as the nonreciprocal versatile interconnections performing the frequency selective regimes of signal propagation in magnonic circuits.

Published under an exclusive license by AIP Publishing. https://doi.org/10.1063/5.0102010

INTRODUCTION

Magnonics is the research field that studies the transport, storage, and processing of data by spin waves (SWs), i.e., the collective excitations of a magnetic material.[1,2] Exploring the third (vertical) dimension in magnonics is a novel and exciting research field driven by the potential for vertically integrated magnonic circuits that takes inspiration from the current development of 3D integrated microelectronics.[3,4] In a recent review book on 3D magnonics[5] as well as in two recent roadmap articles,[6,7] preliminary concepts have been identified, namely, the 3D based peculiar features (e.g., vertical magnon transport, 3D architectures, curvature-induced chiral effects, and nonreciprocal coupling) and related functionalities originating from the interlayer exchange and dipolar coupling between different waveguides and interconnected 3D nanoobjects. This permits the reduction of the power consumption and footprints of magnonic circuits and to design novel

nonlinear effects and functionality unavailable for 2D magnonics. Among 3D magnonic structures, ferromagnetic meander-shaped junctions and waveguides have been proposed as prototypes for the transmission of SW signals in 3D magnonic architectures[8–10] and may have potential applications such as microwave filters, switches, and nonreciprocal devices (isolators and circulators).[11–14] This makes it possible to actively harness the vertical direction for propagating and manipulating SWs, thus overcoming the limitations of SW manipulation and steering in planar magnonic circuits.[15–17] To achieve this goal, detailed knowledge of the magnonic band structure is mandatory to derive information about the frequency ranges where SWs can propagate and how the magnonic bandwidth can be tuned by changing the geometric parameters of the structure.[18–21]

In this work, we investigate experimentally and numerically the dependence of the magnonic band structure on the Ta thickness (t) in $Co_{40}Fe_{40}B_{20}/Ta(t)/Ni_{80}Fe_{20}$ meander-shaped magnetic bilayers. The SWs dispersion (frequency vs wave number-k) is mapped up to the fourth Brillouin zone in the reciprocal space by k-resolved Brillouin light scattering (BLS) spectroscopy and it is calculated by MuMax3 micromagnetic simulations. The measured magnonic band structure contains both stationary and dispersive modes. A significant frequency asymmetry (nonreciprocity) between SWs counterpropagating having opposite signs of their wave number along the periodicity direction is calculated and it is explained in terms of the variation of the dynamic dipolar coupling between the layers for different Ta spacer thickness. Moreover, the lowest three frequency modes increase their frequency and separation by increasing the Ta spacer thickness. This trend is explained by considering the formation of stationary modes in the horizontal segments of the NiFe layer.

SAMPLES AND METHODS

The samples were fabricated on pre-patterned Si (100) substrates into a periodic grating (height $h = 50$ nm, line and trench widths of 300 nm each) by conventional deep-UV photolithography and reactive ion etching. Next, a Ta(2 nm)/$Co_{40}Fe_{40}B_{20}$(15 nm)/Ta (2 nm) stack was deposited by physical vapor deposition (PVD) onto the grating. The length of the horizontal segments was 300 nm, so the unit cell had a periodicity of $a = 600$ nm, corresponding to a Brillouin zone (BZ) edge of $\pi/a = 5.2$ rad μm^{-1}. The limited conformality of the PVD process led to approximately half the film thickness on the vertical segments (sidewalls) with respect to the horizontal ones. After air exposure, a Ta layer of 1, 3, and 8 nm thickness was deposited onto the structure, leading to a total Ta spacer of $t = 3$, 5, and 10 nm, followed by the *in situ* deposition of a 23 nm thick $Ni_{80}Fe_{20}$ magnetic layer. Figure 1 shows (a) a schematic representation of the sample structure and (b) scanning electron microscopy (SEM) images of the CoFeB/Ta(10 nm)/NiFe sample.

BLS spectra from thermally excited SWs were measured in the backscattering configuration using a Sandercock (3 + 3)-pass tandem Fabry–Perot interferometer.[22] An in-plane magnetic field of $\mu_0 H = 50$ mT was applied along the groove length (z-direction) and perpendicular to the incidence plane of light (x–y plane), in the so-called Damon–Eshbach configuration (k perpendicular to applied field). At this field value, the hysteresis loops (not shown)
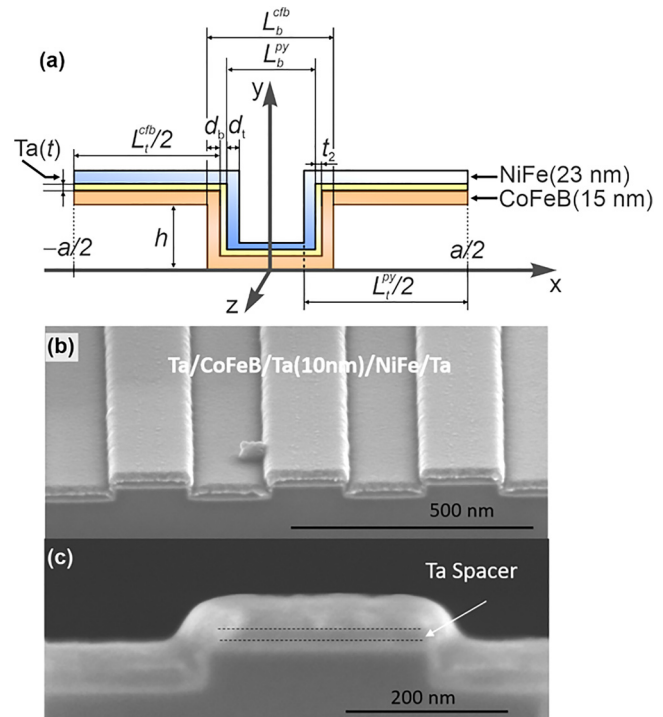

FIG. 1. (a) Schematic geometry and (b) SEM images of CoFeB/Ta(10 nm)/NiFe meander structures showing the uniform thickness of all the deposited layers over a large area as well as their sharp vertical interconnections. (c) Enlarged view of the sample unit cell where the region of the Ta spacer is indicated by the two horizontal dotted lines. All dimensions and geometrical parameters are denoted with symbols that are explained in the text.

indicate that the samples are saturated along the z-direction and we assume the magnetization to be uniform along groove length. SW dispersion was mapped up to the fourth Brillouin zone in the reciprocal space by sweeping the in-plane wave number $k = (4\pi/l) \times \sin(\theta)$ along the x-direction from 0 to $20\,\mu m^{-1}$, where $\lambda = 532$ nm is the laser wavelength and θ is the incidence angle of light.[23]

To model the magnonic band structure of the meander-shaped CoFeB/Ta/NiFe bilayers, micromagnetic simulations were carried out by using the open-source GPU accelerated software MuMax3[24] and performing a 2D Fast Discrete Fourier Transform in time and space. The same method has been described in Refs. 25 and 26 and here we limit ourselves to report the differences with respect to previous studies. To calculate the SW dispersion relation, $N_P = 62$ periods of the meander structure were simulated. Hence, the total length of the simulated structure in the x-direction was $L = N_p \times a = 37.2\,\mu m$. The magnetic bilayer CoFeB/Ta/NiFe meander-shaped unit cell structure was discretized into cubic cells of dimensions $\Delta_x \times \Delta_y \times \Delta_z = 0.5 \times 0.5 \times 0.5$ nm^3. In the $L \times s$ area, where $s = h + d_b + d_t + t$, a rectangular grid with the size of $N_x \times N_y$ was specified, where $N_x = L/\Delta_x$, $N_y = L/\Delta_y$ are the number of grid nodes along the x and y axes, respectively. The width of the vertical segments (sidewalls) is equal to half of the thickness of the

horizontal ones, i.e., $d_b = 7.5$ nm and $d_t = 11.5$ nm for bottom CoFeB and top NiFe layers, correspondingly. Similarly, the nonmagnetic spacer in the vertical section has also half the thickness of the Ta layer thickness in the horizontal section, i.e., $t_2 = t/2$ for all three samples. The magnetic materials were represented in the MuMax3 simulations by the following parameters: saturation magnetizations M_s (CoFeB) = 1275 kA/m, M_s (NiFe) = 800 kA/m, exchange constants A_{ex} (CoFeB) = 1.43×10^{-11} J/m, and A_{ex} (NiFe) = 1.3×10^{-11} J/m. The Gilbert damping value for the CoFeB and Py materials was assumed to be the same and equal to 0.004 that is close to the experimental results obtained earlier by other authors.[27–29]

RESULTS AND DISCUSSION

Figure 2(a) shows BLS spectra measured for the CoFeB/Ta(t)/NiFe samples for different thicknesses of the Ta spacer t at the fixed k magnitude of $4.1 \mu m^{-1}$ and applied field of 50 mT. The spectra are characterized by a significant peak intensity asymmetry when comparing negative (Stokes) and positive (anti-Stokes) frequency shift ranges. Consequently, some peaks are only clearly visible on the Stokes side. This intensity asymmetry prevents us to perform an experimental verification of the nonreciprocal mode character. However, a direct comparison between BLS frequency data and the calculated dispersion enables us to state that a better agreement is achieved when the measured Stokes frequencies are compared to the frequencies of propagating SW along the negative x-direction (k_-). A detailed discussion of the nonreciprocal effects is presented later in the paper.

The three lowest frequency peaks, observed on the Stokes side of the spectra, exhibit an overall frequency increase on increasing

the Ta spacer thickness. The frequency increase reaches about 0.8 GHz for the largest Ta spacer thickness (10 nm). Their calculated frequencies are plotted in Fig. 2(b) as a function of the Ta spacer thickness. The comparison with the frequency data obtained by micromagnetic calculations is shown in Fig. 2(b) and presents a fairly good agreement with experiments. The reason for this monotonic frequency increase is discussed later in the paper.

Figures 3(a)–3(c) present the calculated frequency dispersion for equivalent planar CoFeB(15 nm)/Ta(t)/NiFe(23 nm) magnetic bilayer for wave number in the range from −40 to 40 rad/μm^{-1}. In the present work, due to the large thickness of the Ta nonmagnetic spacer, we focus on the effect of the interlayer dynamic dipolar coupling, only, while the interlayer Ruderman–Kittel–Kasuya–Yosida interaction is neglected.[30,31] Calculated SW frequency dispersion contains two modes with a well-defined phase relation between the dynamic magnetization within the two layers. They correspond to the acoustic mode at a higher frequency and the optic mode at a lower frequency and are associated, respectively, with the in-phase and out-of-phase precession of the dynamic magnetization in the two magnetic layers, respectively.[32–35] The acoustic mode is mainly localized in the bottom CoFeB layer whereas the optic branch has a more pronounced amplitude of dynamic magnetization in the topmost NiFe film.

Moreover, we examine the SW nonreciprocity deriving from the dipolar interaction between the magnetic layers. Noticeably, the optic mode exhibits a larger frequency difference (frequency nonreciprocity) between counterpropagating waves, i.e., for positive (k_+) and negative (k_-) propagation directions, than the acoustic mode. The nonreciprocity increases on increasing the Ta spacer thickness and manifests itself in a large variation of the dispersion slopes for the lowest frequency modes.
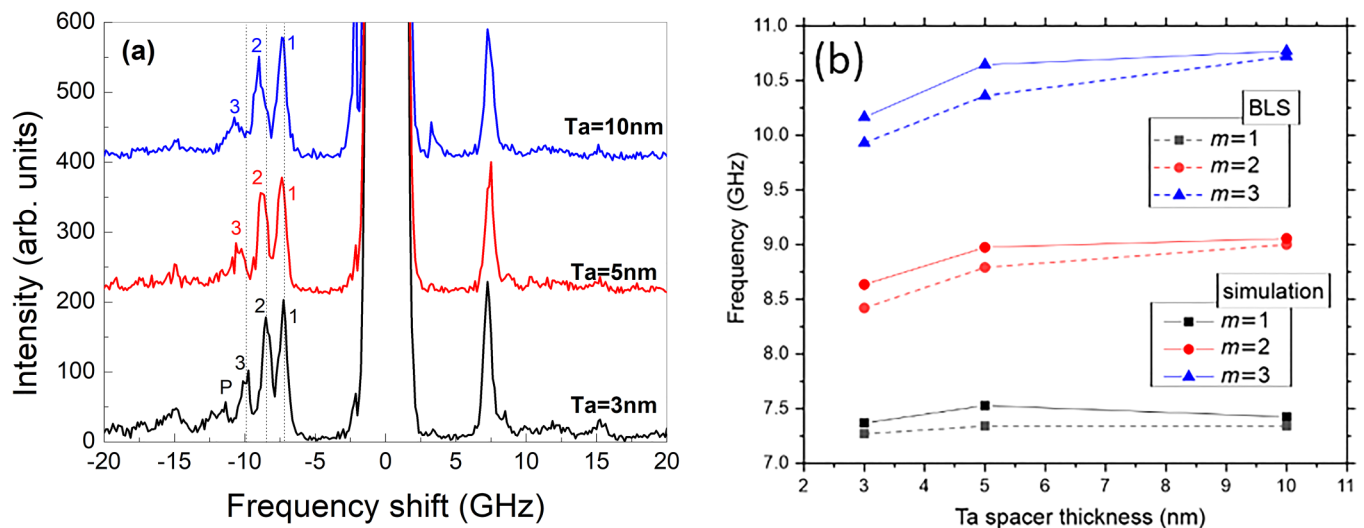

FIG. 2. (a) Experimental BLS spectra and (b) calculated mean frequency of the lowest three spin-wave modes for different values of Ta-spacer thickness t in CoFeB/Ta(t)/NiFe meander structures. Spectra are recorded for a magnetic field of 50 mT applied along the z-axis and $k = 4.1$ rad/μm. The lowest three frequency peaks are labeled as $m = 1$, 2, and 3 while the peak observed for Ta = 3 nm, labeled as P, represents the propagative wave that at this k value is only visible in the measured dispersion of Fig. 3(d).
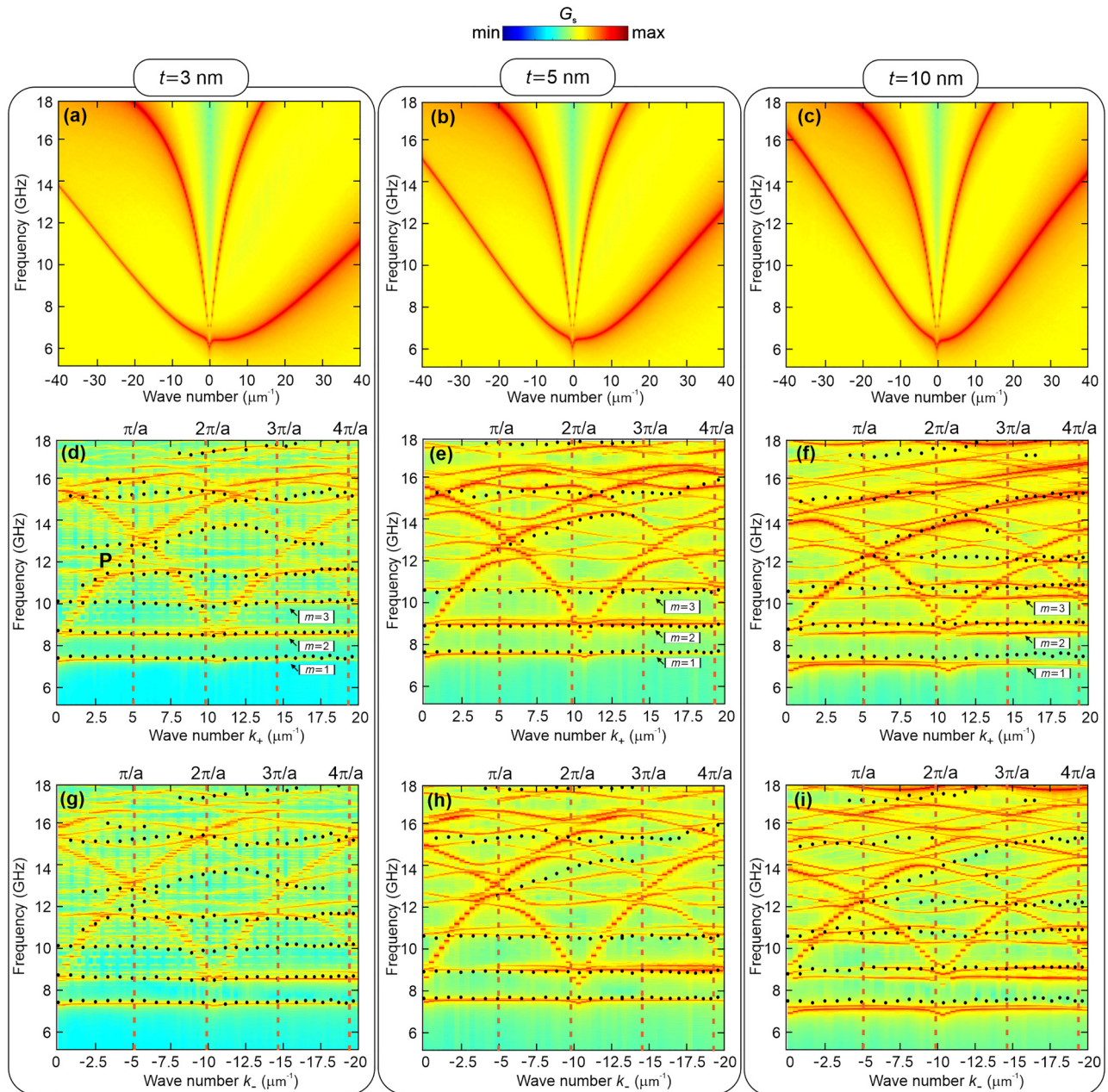
FIG. 3. SW frequency dispersion of an equivalent planar CoFeB/Ta(t)/NiFe magnetic bilayers for $t = 3$ nm (a), $t = 5$ nm (b), and $t = 10$ nm (c). Comparison between measured (points) and simulated (color map) dispersion relations for CoFeB/Ta(t)/NiFe meander sample for propagating SWs along the positive x-direction (k_+) [(d)–(f)] and in negative x-direction (k_+) [(g)–(i)] for different spacer thickness $t = 3$ nm [(d) and (g)], $t = 5$ nm [(e) and (h)], and $t = 10$ nm [(f) and (i)]. In all cases, the external magnetic field was applied along the z-axis and fixed at $\mu_0 H = 50$ mT. The vertical dashed lines mark the edges of the BZs ($n\pi/a$, with $n = 1, 2, 3$, and 4).

Panels (d–i) in Fig. 3 compare the measured (black points) and calculated SW dispersion relations (colored intensity plot) for the CoFeB/Ta(t)/NiFe meander structures while the in-plane SW wave number k was swept along the positive (k_+) and negative (k_-) x-direction. Three stationary modes are observed in the frequency range from 7.5 to 10.5 GHz whose frequency is independent of the k. Moreover, some additional stationary modes are observed at higher frequencies whose frequency depends on the Ta spacer

thickness. Regarding the propagative mode, it is observed for all the investigated samples with some differences that depend on the Ta thickness. For Ta = 3 nm, the mode dispersion has a periodic dispersion that is related to the artificial periodicity of the structure, i.e., its frequency increases reaching a maximum of 13.7 GHz at the edge of the second Brillouin zone followed by a frequency reduction and merging with the stationary mode observed at about 12.7 GHz. The resulting magnonic bandwidth of this mode is about 2.8 GHz. The observed mode crossing and the absence of a bandgap for each mode doublets at $k = n\pi/a = 5.2 \, \mu m^{-1}$ (n is an odd number) are similar to that of CoFeB meander-shaped film uniformly magnetized along the sample grooves[25] and depend on the fact that the sample magnetization is uniformly distributed along groove length (z-axis) and the meander periodicity along the x-direction does not create any periodic magnetization modulation.[36] A slightly different trend is observed for the dispersive more for $t = 5$ nm where it is observed over a limited k-vector range while for $t = 10$ nm its frequency evolution is monotonic up to the edge of the third BZ without periodic oscillation. Above this k-value, a stationary mode at 15.2 GHz is visible only. As a general comment, an overall very good agreement between measured and calculated dispersion relations is observed for both the stationary and dispersive modes.

Regarding the three stationary modes measured in the lowest frequency range of the spectra, calculations indicate that each mode of the triplet is formed by a doublet of modes whose frequency separation increases with m. The calculated average frequency of each doublet of modes $m = 1,2,3$ $[\nu(k_+) + \nu(k_-)/2]$ is shown in Fig. 2(b) as a function of the Ta spacer thickness (t) and compared to the experimental frequency values. The overall tendency for all three doublet modes manifests an increase in the mean frequency with the increase in the nonmagnetic spacer thickness t, which is in good agreement with predictions of micromagnetic simulations. This effect is more pronounced for modes $m = 2$ and $m = 3$ while mode with $m = 1$ does not vary much with the Ta spacer thickness because this mode lies in the region of low group velocities for both branches of the k_+ and k_- dispersion characteristics. As the mode number m increases, SWs propagate at a higher group velocity and the splitting between resonant frequencies increases. It is important to notice that the doublets of peaks are not observed in the BLS spectra probably because of the reduced frequency resolution of the technique.

To explain the frequency evolution of the calculated mode doublets and considering that for low k-vectors ($<20 \, \mu m^{-1}$) the lowest frequency optic mode of the planar bilayer is mainly concentrated in the NiFe layer, we consider the formation of the standing SW modes based on the fulfillment of the wavenumbers condition in the bilayer meander-shaped structure,

$$k_+(\omega_t)L_t^{py} + k_-(\omega_t)L_t^{py} + \varphi_{t+} + \varphi_{t-} = 2\pi n,$$

$$k_+(\omega_b)L_b^{py} + k_-(\omega_b)L_b^{py} + \varphi_{b+} + \varphi_{b-} = 2\pi n,$$

where $k_{+,-}$ is the wavenumbers for SWs propagating in positive and negative x-directions in the bilayer structure, L_t^{py} and L_b^{py} are the length of horizontal top and bottom NiFe segments, $\varphi_{+,-}$ are the phase shifts associated with the SW reflection from both the

vertical sidewalls inside the primitive cell, and n is an integer number. In our particular case, when a SW is incident on the junction between horizontal and vertical segments with $(d_1 > d_2)$, the reflection coefficient $\Gamma = \frac{d_1 - d_2}{d_1 + d_2}$ is positive and the phase shift is zero.[25] Considering this condition in the planar magnetic bilayers, the increase in the frequency splitting in each doublet of modes is explained by taking into account that, for a fixed wave number, an increase of t leads to an increase in the frequency difference (nonreciprocity) of waves propagating in opposite directions $\Delta \nu(k) = \nu(-k) - \nu(k)$, see Figs. 3(a)–3(c), whose origin is due to the dynamic dipolar interactions between ferromagnetic layers and to the magnetic contrast (difference in saturation magnetization) between CoFeB and NiFe.[37,38]

We now consider the origin of splitting inside mode doublets in the meander-shaped bilayer. First, we notice that the calculated frequency separation between each mode of the doublet increases on increasing the Ta spacer thickness reaching the value of 0.5 GHz for the third doublet denoted as $m = 3$ in Figs. 3(f) and 3(i). At the same time, the frequency separation between the modes inside the doublet increases with the number of the doublet. With the decrease in the spacer thickness, both the value of the mean frequency of each mode doublet and the frequency separation are decreased, as seen in Fig. 2(b) and compared to panels (d–i) in Fig. 3. Here, we should note that analysis of BLS data results in one branch depicted by the dots in panels (d–i) in Fig. 3. At the same time, the broadening of the corresponding peaks was observed in the frequency range from 7 to 11 GHz for larger Ta spacer thickness which provides evidence of the multiple peak formation. The latter fact is revealed by micromagnetic simulation. For $t = 3$ nm [Figs. 3(d) and 3(g)], the confluence inside the doublets is visible and these three lower modes are almost dispersionless, i.e., their frequency was independent of the wave number even at the wavenumbers close to $k = n\pi/a$ (n is an even number).

Inspection of Fig. 3 suggests the possible branch crossing between the propagating mode (P) and some of the stationary modes (e.g., $m = 3$) that leads close to the crossing frequency to hybridization of these two modes that may show up as a doublet in the BLS spectra. In a homogeneous magnetic bilayer, there are two branches of the high-frequency and low-frequency modes. For a homogeneous structure, there is no coupling between two waves propagating at the same frequency with different wave numbers [Figs. 3(a) and 3(b)]. As soon as the spatial inhomogeneity arose, then at the transition points between the vertical and horizontal sections, the structure became inhomogeneous. This will lead to the fact that a high-frequency mode wave incident on an inhomogeneous region causes not only reflection and transmission of the high-frequency mode, but also excites low-frequency modes, since they have the same frequency. This occurs in a narrow frequency range only in the vicinity of the intersection of these two branches of high-frequency and low-frequency modes. In this case, we have hybridization of these modes, which is seen in Figs. 3(d)–3(i).

Next, we perform the micromagnetic calculation of the mode spatial profiles for the three lowest frequency doublets of modes observed in the SW dispersion. The normalized dynamic component of magnetization (M_y/M_s) at $k = 0$ (i.e., in the center of the BZ) is shown in Fig. 4. The simulations show that the dynamic
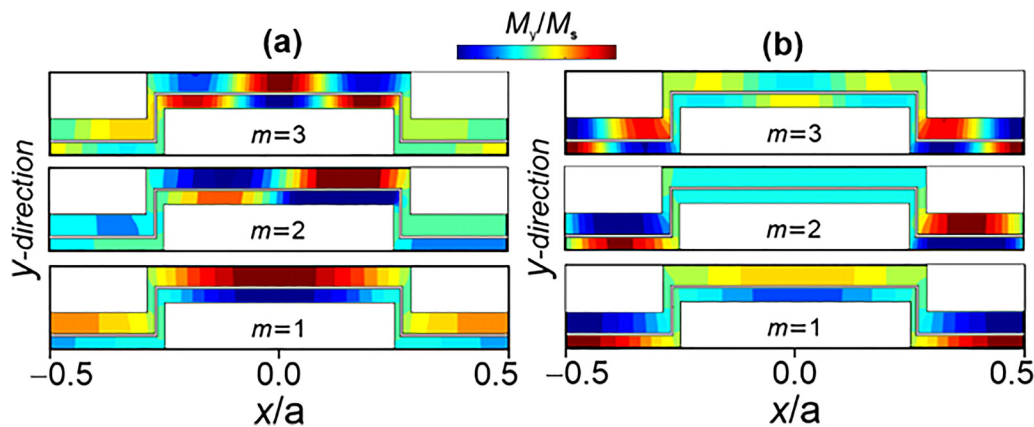
FIG. 4. Simulated spatial profiles (normalized out-of-plane component of dynamic magnetization, M_y/M_s) of the SW modes in CoFeB/Ta(3 nm)/NiFe meander structure for each mode inside doublets: low-frequency (a) and high-frequency (b) modes inside each mth doublet.

magnetization oscillations of low-frequency [Fig. 4(a)] and high-frequency [Fig. 4(b)] modes inside each mth doublet were concentrated both in the topmost NiFe and bottom CoFeB layer with an increasing number of nodes in the horizontal segments with an increase of m. The spatial distributions of low- and high-frequency modes for doublets with $m = 1$ and $m = 3$ were symmetric with respect to the center of the unit cell ($x = 0$), while for the second doublet ($m = 2$) the magnetization profiles are anti-symmetric. At the same time, we notice that the amplitude of the dynamic magnetization is mainly localized in the top and bottom horizontal segments [Fig. 4(a)] while it is less pronounced in the vertical sidewalls, which is well corresponded with the above-mentioned features and explanation of the origin of the mode splitting. Based on this explanation, we suppose that the splitting of the propagated in bilayer meander modes for CoFeB layer is not visible even in the micromagnetic simulation because of the relatively smaller differences between the length of horizontal top L_t^{cfb} and bottom L_b^{cfb} CoFeB segments of the bilayer meander [see Fig. 1(a)].

Finally, the SW nonreciprocal behavior of dispersion in bilayer meander-shape bilayer can be seen in comparison between dispersion plotted in panels (d–i) of Fig. 3 for SW modes propagating along the positive and negative x-directions. This allows us to conclude that the propagating mode localized within the CoFeB layer[26] slightly changes the slope with the variation of the direction of SW propagation, while the split modes for each doublet significantly transform for positive and negative orientation of wave number. This can be explained by the strength of nonreciprocal evidence in SW dispersion for bilayer film for the lower mode [Figs. 3(a)–3(c)]. The slope of the low-frequency branch is significantly modified when compared to the high-frequency one.

In conclusion, we have studied the SW dispersion relation of in-plane saturated CoFeB/Ta/NiFe meander-shaped bilayer structure. On increasing the Ta spacer thickness, the lowest frequency peaks of the spectra increase monotonously in their frequency splitting. The second and third lowest frequency modes increase also concerning their midgap frequency. Calculations indicate that each of these peaks is made of a doublet of modes whose frequency evolution is explained in terms of the nonreciprocal behavior induced by the dynamic dipolar coupling. This could generate a novel class of nonreciprocal on-chip signal processing devices compatible with the existing semiconductor technology and capable of functioning in the absence of a permanent bias magnetic field.

AUTHOR DECLARATIONS

Conflict of Interest

The authors have no conflicts to disclose.

Author Contributions

G. Gubbiotti: Conceptualization (equal); Investigation (equal); Writing – original draft (equal); Writing – review & editing (equal). **A. Sadovnikov:** Formal analysis (equal); Writing – original draft (equal); Writing – review & editing (equal). **S. E. Sheshukova:** Formal analysis (equal); Visualization (equal). **E. Beginin:** Data curation (equal); Methodology (equal); Visualization (equal). **S. Nikitov:** Writing – original draft (equal). **G. Talmelli:** Formal analysis (equal); Validation (equal). **C. Adelmann:** Writing – review & editing (equal). **F. Ciubotaru:** Methodology (equal); Writing – original draft (equal); Writing – review & editing (equal).

DATA AVAILABILITY

The data that support the findings of this study are available from the corresponding author upon reasonable request.

REFERENCES

[1] A. D. Karenowska, A. V. Chumak, A. A. Serga, B. Hillebrands *et al.*, "Magnon spintronics," in *Handbook of Spintronics*, edited by Y. Xu (Springer Science +Business Media, Dordrecht, 2016).

[2] S. M. Rezende, *Fundamentals of Magnonics,* Lecture Notes in Physics (Springer Nature Switzerland AG, 2020).

[3] L. Brunet *et al.*, in *IEEE Symposium on VLSI Technology*, Honolulu, HI, USA, *2016* (IEEE, 2016), Vol. 1.

[4] A. Vandooren *et al.*, in *IEEE Symposium on VLSI Technology*, Honolulu, HI, *2018* (IEEE, 2018), Vol. 69.

[5] G. Gubbiotti, *Three-Dimensional Magnonics* (Jenny Stanford, Singapore, 2019).

[6] A. Barman *et al.*, J. Phys. Condens. Matter. **33**, 413001 (2021).

[7] A. V. Chumak *et al.*, IEEE Trans. Magn. **58**, 0800172 (2022).

[8] V. K. Sakharov, E. N. Beginin, Y. V. Khivintsev, A. V. Sadovnikov, A. I. Stognij, Y. A. Filimonov, and S. A. Nikitov, Appl. Phys. Lett. **117**, 022403 (2020).

[9] A. A. Martyshkin, E. N. Beginin, A. I. Stognij, S. A. Nikitov, and A. V. Sadovnikov, IEEE Magn. Lett. **10**, 5511105 (2019).

[10] E. N. Beginin, A. V. Sadovnikov, A. Y. Sharaevskaya, A. I. Stognij, and S. A. Nikitov, Appl. Phys. Lett. **112**, 122404 (2018).

[11] O. Gladii, M. Haidar, Y. Henry, M. Kostylev, and M. Bailleul, Phys. Rev. B **93**, 054430 (2016).

[12] R. A. Gallardo, T. Schneider, A. K. Chaurasiya, A. Oelschlägel, S. S. P. K. Arekapudi, A. Roldán-Molina, R. Hübner, K. Lenz, A. Barman, J. Fassbender, J. Lindner, O. Hellwig, and P. Landeros, Phys. Rev. Appl. **12**, 034012 (2019).

[13] P. Roberjot, K. Szulc, J. W. Kłos, and M. Krawczyk, Appl. Phys. Lett. **118**, 182406 (2021).

[14] K. Szulc, P. Graczyk, M. Mruczkiewicz, G. Gubbiotti, and M. Krawczyk, Phys. Rev. Appl. **14**, 034063 (2020).

[15] K. Vogt, F. Y. Fradin, J. E. Pearson, T. Sebastian, S. D. Bader, B. Hillebrands, A. Hoffmann, and H. Schultheiss, Nat. Commun. **5**, 3727 (2014).

[16] J. Stigloher, M. Decker, H. Körner, K. Tanabe, T. Moriyama, T. Taniguchi, H. Hata, M. Madami, G. Gubbiotti, K. Kobayashi, T. Ono, and C. H. Back, Phys. Rev. Lett. **117**, 037204 (2016).

[17] A. Haldar and A. O. Adeyeye, Appl. Phys. Lett. **119**, 060501 (2021).

[18] J. Topp, D. Heitmann, M. P. Kostylev, and D. Grundler, Phys. Rev. Lett. **104**, 207205 (2010).

[19] V. L. Zhang, H. S. Lim, C. S. Lin, Z. K. Wang, S. C. Ng, M. H. Kuok, S. Jain, A. O. Adeyeye, and M. G. Cottam, Appl. Phys. Lett. **99**, 143118 (2011).

[20] G. Gubbiotti, S. Tacchi, M. Madami, G. Carlotti, S. Jain, A. O. Adeyeye, and M. P. Kostylev, Appl. Phys. Lett. **100**, 162407 (2012).

[21] A. De, K. Dutta, S. Mondal, S. Barman, Y. Otani, and A. Barman, Phys. Rev. B **103**, 064402 (2021).

[22] J. R. Sandercock, *Light Scattering in Solids III*, Springer Series in Topics in Applied Physics Vol. 51, edited by M. Cardona and G. Guntherodt (Springer-Verlag, Berlin, 1982), p. 173.

[23] G. Carlotti and G. Gubbiotti, J. Phys.: Condens. Matter. **14**, 8199 (2002).

[24] A. Vansteenkiste and B. Van De Wiele, J. Magn. Magn. Mater. **323**, 2585 (2011).

[25] G. Gubbiotti, A. Sadovnikov, E. Beginin, S. Nikitov, D. Wan, A. Gupta, S. Kundu, G. Talmelli, R. Carpenter, I. Asselberghs, I. P. Radu, C. Adelmann, and F. Ciubotaru, Phys. Rev. Appl. **15**, 014061 (2021).

[26] G. Gubbiotti, A. Sadovnikov, E. Beginin, S. Sheshukova, S. Nikitov, G. Talmelli, I. Asselberghs, I. P. Radu, C. Adelmann, and F. Ciubotaru, Appl. Phys. Lett. **118**, 162405 (2021).

[27] R. O'Handley, R. Hasegawa, R. Ray, and C.-P. Chou, Appl. Phys. Lett. **29**, 330 (1976).

[28] C. Bilzera, T. Devolder, J.-V. Kim, G. Counil, and C. Chappert, J. Appl. Phys. **100**, 053903 (2006).

[29] X. Liu, W. Zhang, M. J. Carter, and G. Xiao, J. Appl. Phys. **110**, 033910 (2011).

[30] P. Grunberg, R. Schreiber, and Y. Pang, Phys. Rev. Lett. **57**, 2442 (1986).

[31] Y. A. Filimonov, G. T. Kazakov, S. L. Visotsky, B. P. Nam, and A. S. He, J. Magn. Magn. Mater. **131**, 235 (1994).

[32] P. Grunberg and K. Mika, Phys. Rev. B. **27**, 2955 (1983).

[33] J. Barnas and P. Grunberg, J. Magn. Magn. Mater. **82**, 186 (1989).

[34] J. J. Krebs, P. Lubitz, A. Chaiken, and G. A. Prinz, Phys. Rev. Lett. **63**, 1645 (1989).

[35] G. Gubbiotti, M. Kostylev, N. Sergeeva, M. Conti, G. Carlotti, T. Ono, A. N. Slavin, and A. Stashkevich, Phys. Rev. B **70**, 224422 (2004).

[36] F. Montoncello and G. Gubbiotti, Sci. Rep. **11**, 21344 (2021).

[37] P. A. Grünberg, Rev. Mod. Phys. **80**, 1531 (2008).

[38] M. S. Sodha and N. C. Srivastava, "Plane waves in ferrimagnetics," in *Microwave Propagation in Ferrimagnetics* (Springer, Boston, MA, 1981).